Chemistry and Materials Research
ISSN 2224- 3224 (Print) ISSN 2225- 0956 (Online)
Vol.3 No.13, 2013

Structural and Optical Properties of Tin Doped Zinc Oxide Fibres Prepared By Electrospinning Technique

E. D. Adelowo [1]*, A. Y. Fasasi [2], M.O. Adeoye [3], S. O. Alayande [4]
[1]Department of Materials and Metallurgical Engineering, Federal University, Oye-Ekiti, Ekiti State, Nigeria
[2,4]Centre for Energy Research and Development, Obafemi Awolowo University, Ile-Ife, Osun State, Nigeria
[3]Department of Materials Science and Engineering, Obafemi Awolowo University, Ile-Ife, Osun State, Nigeria
*E-mail of the corresponding author: ezdotsm@gmail.com

ABSTRACT

The study synthesized ZnO fibers using electrospinning technique. It also characterized and determined the effects of Sn^{2+} dopant on the optical properties of the fibers synthesized. This was with a view to exploring the potential of improving the performance ZnO semiconductor material in industrial applications.

Polyvinyl Alcohol (PVA) solution was prepared and mixed with ZnO source. Zinc acetate was used as the ZnO source while Tin Acetate was used as Sn^{2+} dopant source. Viscous electrospinning solutions of PVA/Zinc Acetate and three different compositions of Tin Acetate were prepared. The compositions of dopants used were 5, 7 and 9-wt. %. Samples of the depositions from the electrospinning process were annealed at 600^{o} C at a rate of 4^{o} C per minute for 6 hours. Scanning electron microscopy (SEM) was employed to reveal the morphology of the depositions. The structural analysis of the fibers was carried out using x-ray diffractometry (XRD) while the optical properties of the fibers were investigated using ultra violet visible spectrophotometry.

The SEM results showed the depositions to be web of fibers. The XRD confirmed the crystallization of undoped and doped ZnO fibers from the acetates. The crystal sizes of the fibers were in the range of 5.566 to 7.202 nm. Furthermore, wide bandgap energy values ranging from 3.26 to 3.46 eV were obtained from the results of the optical properties of the fibers. The results showed that the average crystal sizes of Sn^{2+} doped ZnO fibers were larger than those of the undoped fibers. However, it was observed that the average crystal size decreases with increase in Sn^{2+} content. The results also showed that the bandgap energy values of the fibers increase with dopant concentration.

The study established the viability of fabricating doped and undoped ZnO structure in form of fibers in order to enhance its performance in industrial applications. Also, the results showed that the optical properties of the fibers improved with increase in Sn^{2+} dopant concentration.

Keywords: ZnO fibers; Electrospinning technique; Structural analysis; Optical properties; Sn^{2+} Dopant; Band gap energy value; Crystal size

1. INTRODUCTION

ZnO is a wide bandgap (3.2eV) semiconductor material. It plays a major role in several technologies. The success of ZnO in many applications can be connected to its ability to act as host to a wide variety of dopants. Incorporation of dopants in ZnO systems produce properties useful in several applications such as transparent electrodes in liquid crystal displays, in energy-saving or protecting windows, thin film transistors, gas sensors, solar cells and photodiodes (Hernandez et al 2008; Shan et al 2003). In order to improve the performance of ZnO in existing applications or tailor its properties towards new applications, many research groups have found interest in doping it with impurities of various types and compositions.

Also, the performance of semiconductor based devices has been reported to be strongly connected to the specific surface area of the semiconducting material (Gopel, 1995). A higher specific surface area of semiconductor material leads to improved performance of the device. Many techniques have therefore been adopted to increase the surface area of semiconductor materials. ZnO nanostructures synthesized into fibres have received considerable attention from researchers because of the resulting high specific surface area which gives rise to improved performance. ZnO fibre is produced using various methods such as drawing (Ondarcuhu and Joachim, 1998) , template synthesis (Feng et al, 2002), phase separation (Ma and Zhang, 1999), self assembly (Liu et al, 1996, 1999; Yan et al, 2001; de Moel et al. 2002 and Hartgerink et al, 2001) and electrospinning (Reneker et al, 2000; Chen et al, 2001; Suthar and Chase 2001; Huang et al, 2003; Lim et al, 2004 and Yang et al, 2005). Electrospinning is a special case of the electrospray process which uses an electrostatic field to form and

accelerate liquid jets from the tip of a needle (Reneker et al, 2000; Shin et al, 2001).Electrospinning is an efficient, relatively simple and low cost way to produce polymer and composite fibers with diameters ranging from several nanometers to a few micrometers by applying a high voltage to a polymer solution or melt ejected from a spinneret or needle (Reneker et al, 1996; Doshi et al 1995; Fong et al 1999).

The purpose of this work is to evaluate the structural and optical properties of pure and Sn doped ZnO fibres fabricated using electrospinning method. In this study, pure ZnO and a range of compositions of $Sn_xZn_{1-x}O$ were electrospun into fibres. The formation of the fibers was confirmed using Scanning Electron Microscopy (SEM) and the structural and optical properties were then evaluated.

2. EXPERIMENTAL

The electrospinning set-up consists of a spinneret, a high-voltage (5 to 50 kV) direct current power supply, an aluminium foil as collector and glass slides as substrates. Poly Vinyl Alcohol (PVA) solution was prepared by dissolving 1.5 g of PVA powder in 10 ml of distilled water followed by heating at 80^{o}C and stirring for 1 hour to obtain a homogeneous viscous PVA solution. Zinc acetate (1 g) was dissolved in 8 ml of distilled water and added to the PVA solution. The resulting solution was then stirred for 2 hours to obtain a viscous PVA/zinc acetate electrospinning solution.

Zinc acetate salt (1g) was dissolved in 8ml of distilled water followed by addition varying amount of tin acetate. The resulting solution of zinc acetate and tin acetate was mixed with PVA solution to give 5 wt. %, 7 wt. % and 9 wt. % Sn^{2+} doping of the PVA/zinc acetate followed by stirring for 2 hours to produce a viscous PVA/zinc acetate/tin acetate electrospinning solution.

Each of the electrospinning solutions prepared were loaded in the spinneret and one electrode of a high voltage DC generator, was attached to it through a thick copper wire. The other electrode was connected to the aluminium foil collector. The distance between the tip of the spinneret and collector was maintained at 10 cm. A constant voltage of 25 kV was applied to the solution and depositions were collected on glass slides attached to the aluminium foil. For conversion of the acetates to oxides and the removal of polymer (PVA) from the fibres produced, the depositions obtained were annealed in a tubular furnace at 600^{o}C at a rate of 4^{o}C m^{-1} for 6 hours.

The morphology of the deposited fibers were investigated using an EVO-6700 F scanning electron microscope. The structural properties of the fibres were investigated using XRD patterns recorded for the samples by a Radicon MD-10 x-ray diffractometer, using a monochromatized X-ray beam having CuKα radiation with λ = 1.5406 Å (40 mA, 45 kV). A continuous scan mode was used to collect 2θ data from 4° to 72°. The average dimensions of crystallites were determined by the Scherrer's method. The optical properties of the samples were investigated using Perkin Elmer Scan-Lambda 750 double-beam ultraviolet-visible spectrophotometer.

3. RESULTS AND DISCUSSION

3.1. Morphology of the fibers

This section presents results of scanning electron microscopy (SEM) studies. The SEM images confirmed that the product obtained were indeed an assembly of fibers. Typical SEM images of the undoped PVA/zinc acetate fibres unannealed and after annealing at 600^{o}C are presented and discussed. The SEM photographs in plates 1 and 2 show the results of undoped PVA/zinc acetate fibers in unannealed (as-prepared) and annealed form. The images show the general morphology of PVA/zinc acetate fibers. It can be seen that the as-prepared fibers are larger in diameter than the annealed fibers. The as-prepared fibers have average diameter in the range of 200nm while the annealed fibers have diameters around 100nm. The larger diameter observed in the as-prepared fibers can be thought of as a result of the presence of PVA and the acetate group. The diameter of the fibers obtained after annealing at 600^{o}C became smaller due to the removal of both PVA and the acetate group from the zinc acetate molecule. It can also be seen that the surface of the as-prepared fibers is smoother than that of the annealed fibers. The shrinkage of the fibers as a result of the removal of the PVA and acetate group component upon annealing at 600^{o}C is believed to be responsible for the rough surface of the annealed fibers. It is believed that the fibers retained their form but shrank after annealing at 600^{o}C and appear to consist of interconnected particles.

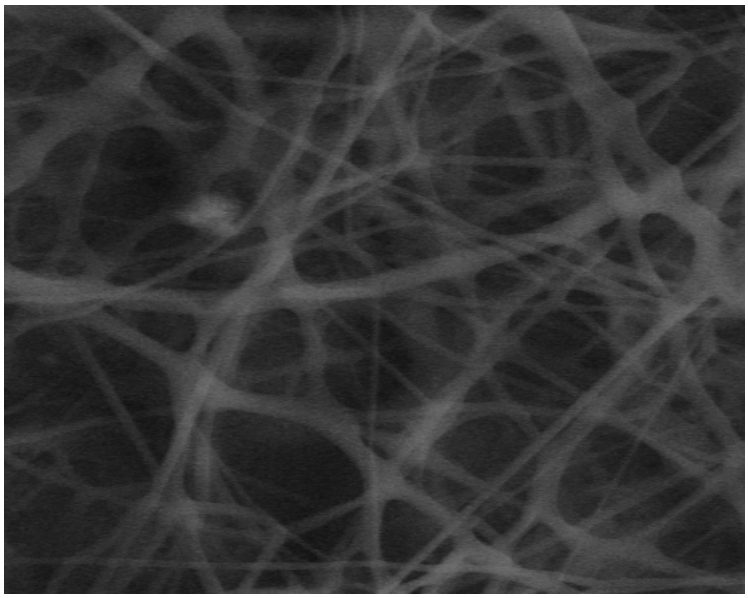

Plate 1: SEM image of electrospun PVA/zinc acetate fibres (1000X)

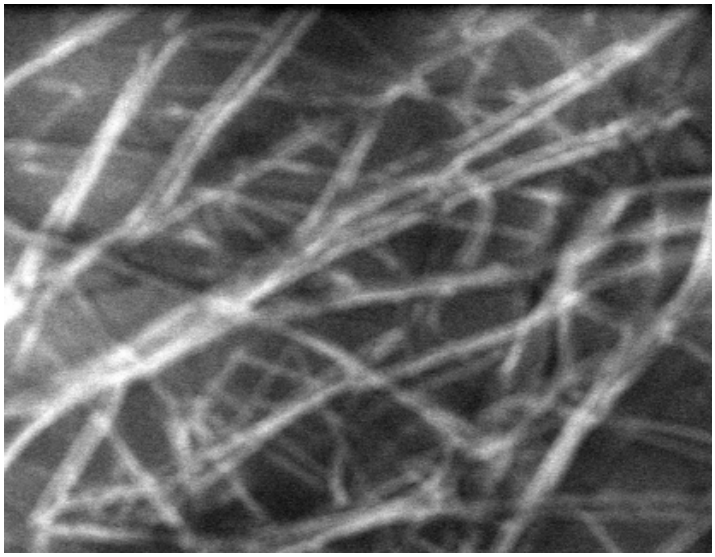

Plate 2: SEM image of electrospun PVA/zinc acetate nanofibres after annealing at 600^{o}C (1000X)

3.2. Structural studies of the fibres

This section presents the structural properties of the fibres obtained using x-ray diffractometry. The XRD spectra were presented for both the Sn^{2+} doped and undoped PVA/zinc acetate fibres. The XRD pattern of the annealed PVA/zinc acetate fibres is shown in Figure 2. The sample was scanned between 2θ angles of 4^{o} and 72^{o} where θ is the angle of incidence of the X-ray beam. Three distinct peaks were observed on the XRD pattern at angles 2θ = 31.97^{o}, 34.75^{o}, and 36.65^{o} which can be indexed as (1010), (0002), and (1011) planes of the hexagonal structure of ZnO (JCPDS card 36-1451). The peaks observed in the pattern reveal the polycrystalline nature of the annealed fibres. The result indicates that ZnO crystallized from the zinc acetate precursor after annealing at 600^{o}C. The XRD pattern corresponding to ZnO fibres doped with varying amount of Sn^{2+} is shown in Figures 2 to 5. Considering the pattern of 5-wt. % Sn^{2+} dopant content (Figure 3), three distinct peaks were observed at 2θ positions 30.85, 34.01 and 36.02 also revealing the polycrystallinity of the fibres. The XRD spectra obtained for

both 7-wt. % and 9-wt. % doped ZnO fibres presented in Figures 4 and 5 exhibit peaks with positions comparable to the 5-wt% Sn^{2+} dopant.

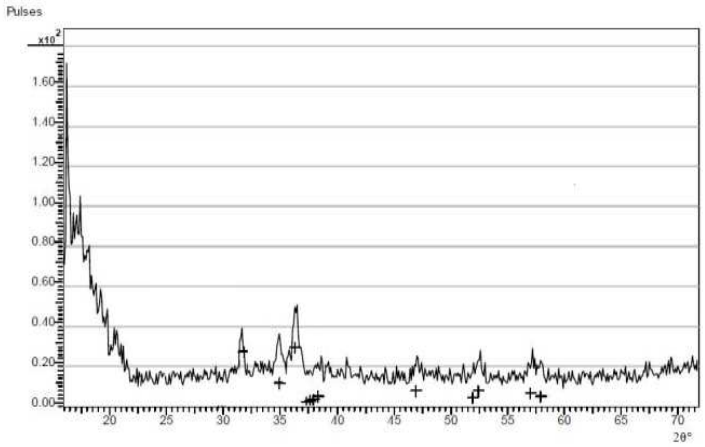

Figure 2: XRD pattern of undoped ZnO fibres.

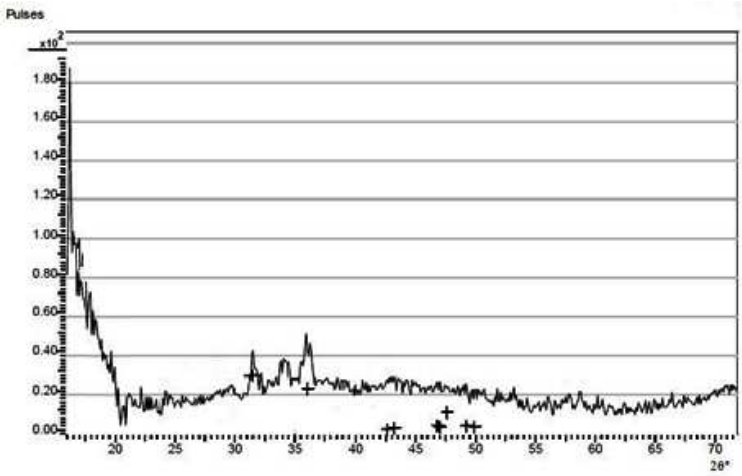

Figure 3: XRD pattern of 5-wt. % Sn^{2+} doped ZnO fibres.

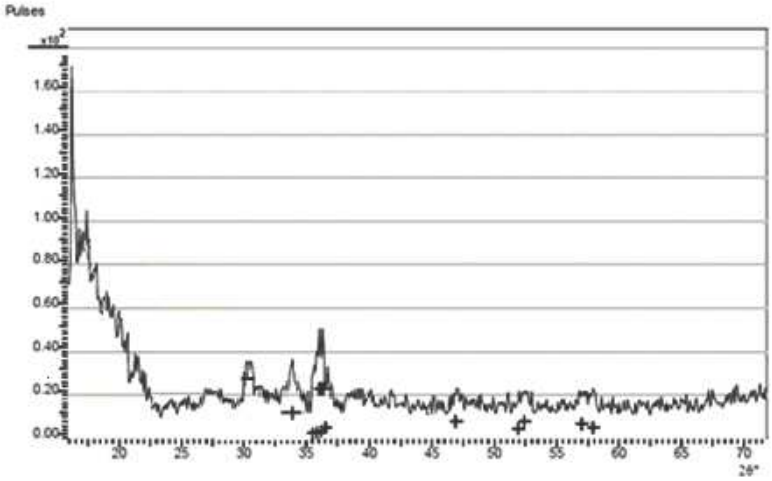

Figure 4: XRD pattern of 7-wt. % Sn^{2+} doped ZnO fibres

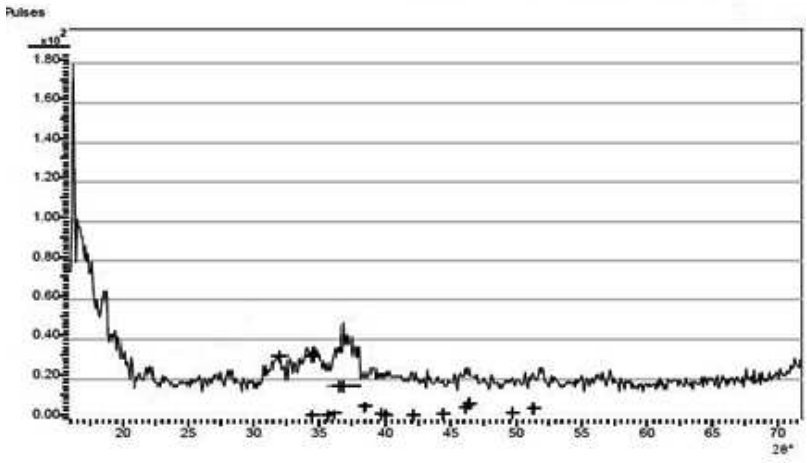

Figure 5: XRD pattern of 9-wt. % Sn^{2+} doped ZnO fibres.

content. It can also be observed that the peaks slightly broadens with increase in Sn^{2+} dopant content. Clearly, in contrast with undoped ZnO fibres, the peak positions of the Sn^{2+} doped samples shifted towards lower values indicating that the lattice arrangement of the ZnO host has been affected by the Sn^{2+} dopant.

The average crystal size of the undoped and Sn^{2+} doped ZnO fibres were estimated by the Debye-Scherrer's formula

$$D = \frac{0.9\lambda}{\beta\cos\theta} \qquad 1$$

where D is the crystal size, λ is the wavelength of the incident X-ray (1.5406), β is the FWHM and θ is the angle at which the maximum peak occurs (Aggarwal et al., 2012). The results obtained were presented in Table 1.

Table 1: Estimates of the average size of the crystals of undoped and Sn^{2+} doped ZnO fibres

ZnO fiber samples	D(nm)
Undoped	5.566
5-wt. % Sn^{2+} doped	7.202
7-wt. % Sn^{2+} doped	7.200
9-wt. % Sn^{2+} doped	7.120

The average crystal sizes of all the Sn^{2+} doped ZnO fibres are higher than that of the undoped fibres. This can be thought of as the effect incorporation of bigger radius Sn^{2+} than Zn^{2+} into the ZnO structure. However, it can be

observed that the average crystal size decreases with increase in Sn^{2+} content. It is believed that the packing density of the crystals of the fibres increased as Sn^{2+} dopant content increased due to gradual disappearance of gaps within the crystals.

The formation of ZnO structure during annealing can be viewed as a two step process of nucleation and growth. During annealing, active nuclei are generated which then grow into the ZnO structure. The growth of the ZnO nanostructure therefore depends on the number of active nuclei produced during annealing. It is believed that the substitution of smaller Zn^{2+} having a radius of 0.74 A^o by a bigger Sn^{2+} with an approximate radius of 1.18 A^o significantly affected the lattice arrangement of the ZnO structure causing distortions. Doping is considered to be the main factor that causes the lattice distortion of crystals, resulting in the development of strain in the unit cell (Huang et al., 2003). It is generally established that strain arises from lattice mismatch and distortion.

The broadening of the peaks in the XRD spectra of Sn^{2+} doped ZnO fibres is attributed to the distortion of the lattice of the ZnO host due to the incorporation large radius Sn^{2+} (1.18A^o) causing the development of strain in the crystal of the ZnO structure. Shifts of XRD peak positions to lower angles as a result of incorporation of dopants has been observed by Singh (2010) in Mn^{2+} (r^{2+}_{Mn} =0.8A^o) doped ZnO nanocrystals. Similarly, the diffraction peaks of Ce^{2+}-doped ZnO nanorods reported by Lang et al. (2010) shifted toward lower angles and it was concluded to be an indication of a little larger lattice parameters than those of undoped ZnO nanorods. The ionic radius of Ce^{4+} (0.92 Å) is much bigger than that of Zn^{2+} (0.74Å).The result may be regarded as an indication of the dependence of resulting lattice parameters on the dopant size and a further confirmation of the actual incorporation of the Sn^{2+} into ZnO structure.

3.3. Optical studies of the fibres

The transmittance of the undoped ZnO fibres as shown in Figure 6 is about 75% with absorption edge around 377nm. All the Sn^{2+} doped ZnO fibres show a higher transmittance than the undoped fibres with an average value of about 85% as shown in Figures 7 to 9. The absorption edge in addition, varies with the amount of Sn^{2+}. The absorption edge for 5-wt. % Sn^{2+} doped fibres was around 376 nm while the absorption edge of the 7-wt. % Sn^{2+} doped fibres was found around 369 nm wavelength. The absorption edge shifted to a lower wavelength around 362 nm on further increasing the Sn^{2+} content to 9-wt. %.

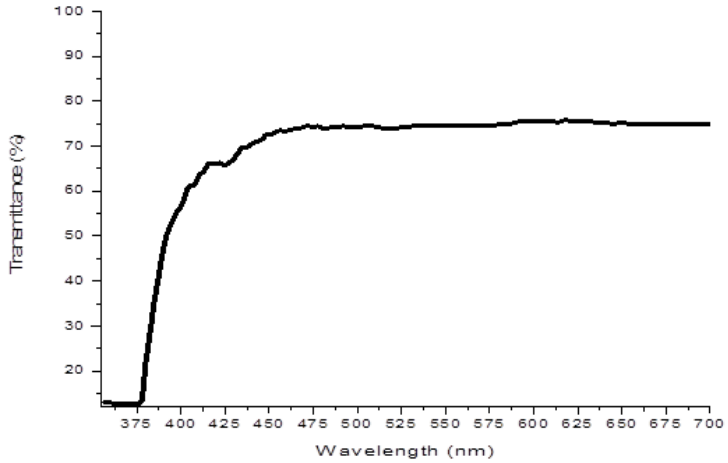

Figure 6: Transmission pattern of undoped ZnO fibres

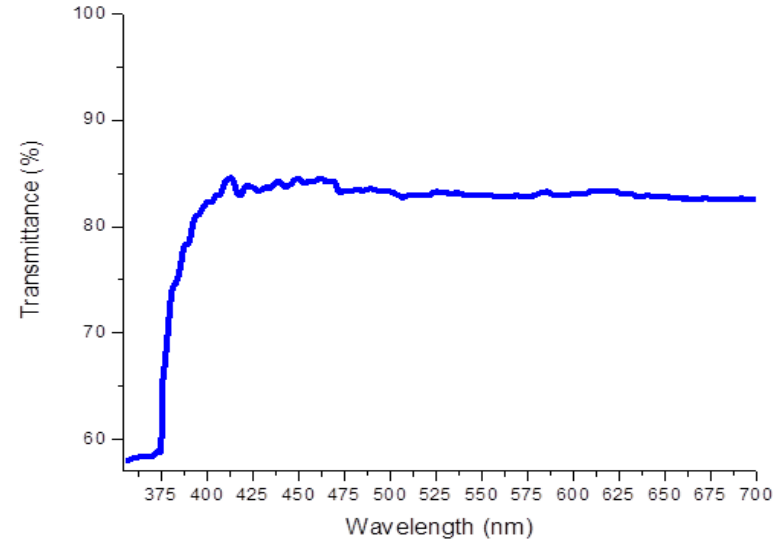

Figure 7: Transmission pattern of 5-wt.% Sn^{2+} doped ZnO fibres

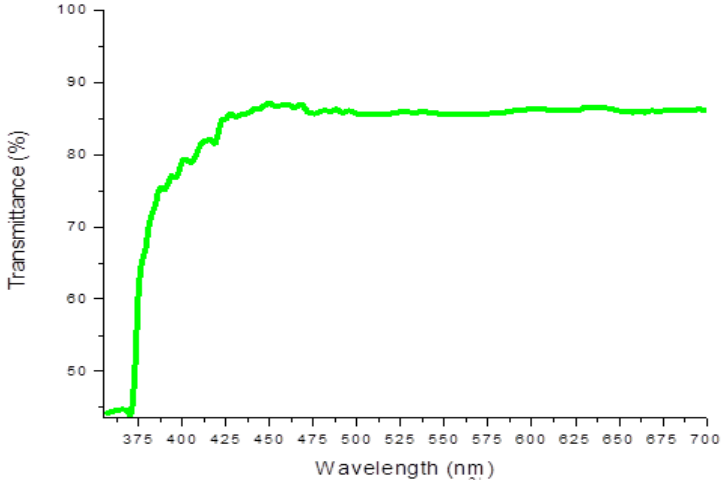

Figure 8: Transmission pattern of 7-wt.% Sn^{2+} doped ZnO fibres

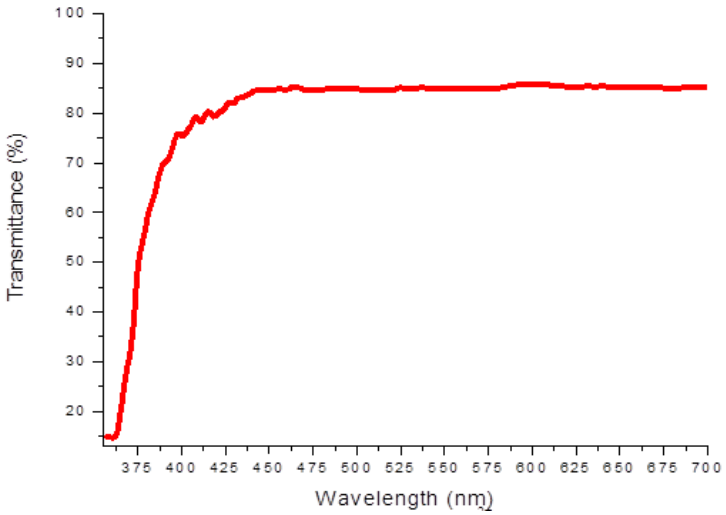

Figure 9: Transmission pattern of 9-wt.% Sn^{2+} doped ZnO fibres

The bandgap energy Eg, can be estimated using the conventional Tauc equation

$$\alpha h\nu = A(h\nu - E_g)^{1/2} \quad (2)$$

Where A is an empirical constant. The bandgap energy of the fibres can be obtained from the zero-crossing value of the extrapolation of a linear fit to the edge of the $(\alpha h\nu)^2$ versus $h\nu$ plot as shown in Figure 10 for undoped ZnO fibres (Pradhan and Leung, 2008). The photon energy is $h\nu$ and α (= -ln T) is the absorbance. The corresponding estimated bandgap energy values of the fibres are summarized in Table 2.

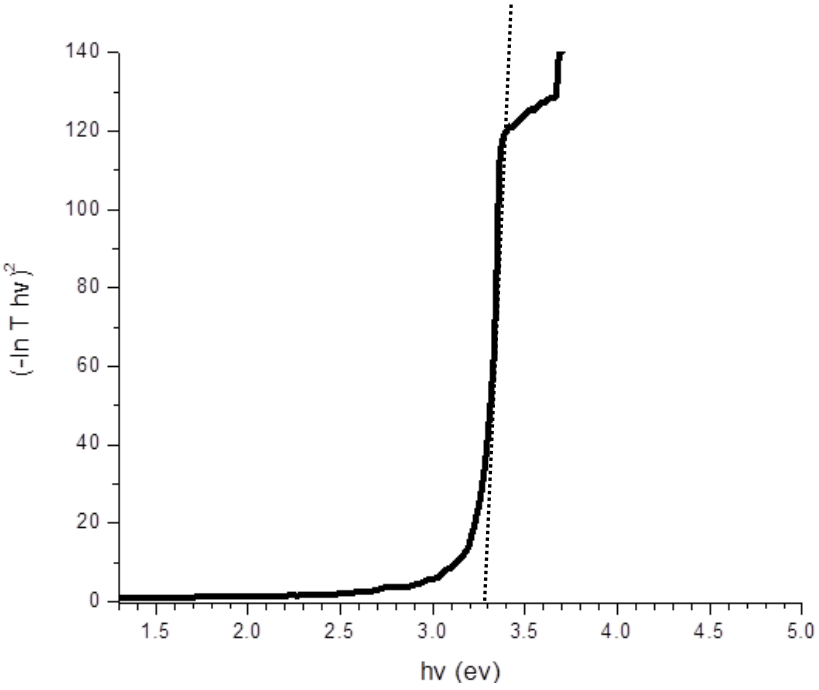

Figure 10: Estimation of bandgap energy of undoped ZnO fibers

Table 2: Bandgap energies of the fibres

ZnO Fiber sample	Bandgap energy, E_g (eV)
undoped	3.26
5-wt. % Sn^{2+} doped	3.32
7-wt. % Sn^{2+} doped	3.35
9-wt. % Sn^{2+} doped	3.46

The bandgap energy obtained for 5-wt. % Sn^{2+} doped ZnO (3.32eV) fibres is higher than that of the undoped ZnO fibres (3.26eV) as presented. The bandgap energy increased to a value of 3.35 eV and 3.46 eV on increasing the Sn^{2+} dopant content to 7-wt. % and 9-wt. % respectively. Clearly, the bandgap energies increase with increase in Sn^{2+} dopant content. The variations observed in the bandgap energies as a result of the amount of Sn^{2+} can be attributed to changes in the size of the crystals of the fibres. It has been observed and discussed earlier that the crystal size estimates obtained from the XRD data for the Sn^{2+} doped ZnO fibres decreases with increasing Sn^{2+} content. The quantum confinement effect provides the basis of a qualitative understanding in the bandgap with a decrease in crystal size. A crystal behaves as if it were free when the confining dimensions is large compared to the wavelength of the crystal. Its kinetic energy can only have discrete values that are

determined by the mass of the crystals and the dimension of the space. During this state, the bandgap remains at its original energy as a result of continuous energy state. As the confining dimension decreases to nanoscale dimensions, the energy pattern becomes discrete. As a result, the bandgap energy becomes size dependent. The confinement of charge carrier (electron and holes) within the restricted dimension of small crystals produces an increase in energy difference of their bandgaps. With this idea it is expected that the properties of the charge carriers in semiconductor materials will exhibit size dependence when crystal dimensions become very small. The increase in bandgap can therefore be understood in terms of an increase in quantum confinement upon crystal size reduction. It is however important to note that the bandgap energy values of Sn^{2+} doped ZnO fibres is higher than that of the undoped fibres despite having larger crystal size. This behaviour may be attributed to the partial filling of the conduction band of the ZnO nanostructure due to doping. ZnO is naturally n-type material and the Fermi level will be inside of the conduction band, when it is doped, the lowest states of the conduction band will be partially filled, due to the increase of carrier concentration. The partial filling of the conduction band leads to a blocking of the lowest states and hence an increase in the optically observed bandgap energy. This increase of the bandgap energy due to doping is generally attributed to the Burstein-Moss effect (Caglar et al., 2006). These observations indicate that bandgap energy depends not only on average crystal size of the ZnO fibres, but also on the influence of dopant composition in the ZnO structure.

4. CONCLUSION

The structural and optical properties of Sn incorporated ZnO fibres prepared by electrospinning were studied in this paper. The XRD measurement used for the structural analysis confirmed the prepared fibres to be ZnO. The XRD data also indicated a shift of the positions of the peaks to lower wavelengths for Sn^{2+} doped ZnO fibres. This was believed to be due to lattice distortions and strains caused by the incorporation of Sn^{2+} with a bigger ionic radius than Zn^{2+} in the ZnO structure thereby retarding its growth. The optical characterisation showed variations in the bandgap energy of the doped ZnO fibres with varying dopant composition. These variations were attributed to both crystal size of the fibres and the level of doping. As the crystal size decreases the quantum effect improves leading to an increase in the bandgap energy. Also, as the doping level increases the observed bandgap energy increases. This increase in bandgap energies with increase in doping level was associated to the Burstein-Moss effect. The wide bandgap energies obtained for all the ZnO fiber samples may make them useful for optical gas sensor application.

REFERENCES

Aggarwal, N., Anand, V.K., Walia, K, Sood S. C., (2012). Structural and Optical Properties of Pure &Aluminium Doped ZnO Thin Films Prepared by Sol-Gel *TECHNIA – International Journal of Computing Science and Communication Technologies*, 4 (2): 09743375.

Caglar, Y., Zor M., Caglar M. And Ilican, S. (2006). Influence of the indium incorporation on the structural and electrical properties of zinc oxide films . *Journal of Optoelectronics and Advanced Materials* Vol. 8 (5) 1867 – 1873.

de Moel, K, van Ekenstein, G.O.R.A., Nijland, H., Polushkin, E., ten Brinke, G., Maki Ontto, R. and Ikkala, O.,(2001). Polymeric nanofibers prepared from self organized supramolecules . Chem. Mater., 13(12), pp. 4580-4583.

Doshi, J.; Reneker, D. (1995). Electrospinning process and applications of electrospun fibers. *J. Electrost.*, 35, 151-160.

Feng, J.J., (2002). The stretching of an electrified non-Newtonian jet: A model for electrospinning . *Phys. Fluids*, 14(11), pp. 3912-3926.

Fong, H.; Chun, I.; Reneker, D. (1999). Beaded nanofibers formed during electrospinning. *Polymer* , 40, 4585-4592.

Gopel, W., (1995). Supramolecular and polymeric structures for gas sensors . *Sens. Actuat. B-Chem*, 24 17-32

Hernandezbattez, A; Gonzalez, R; Viesca, J; Fernandez, J; Diazfernandez, J; MacHado, A; Chou, R; Riba, J., (2008). CuO, ZrO_2 and ZnO nanoparticles as antiwear additive in oil Lubricants. *Wear* 265 (3–4): 422

Hartgerink, J.D., Beniash, E. and Stupp, S.I. (2001). Self-assembly and mineralization of peptide-amphiphile nanofibers. *Science*, 294(5547), pp. 1684-1688.

Huang, Y., M. Liu, Z. Li, Y. Zeng and S. Liu, (2003). Raman spectroscopy study of ZnO-based ceramic films fabricated by novel sol-gel process . *Mater.Sci. Eng.*, B97: 111-116.

Lang, J., Han, Q., Yang J., Li C.,Li X., Yang, L.,Zhang, Y., Gao, M., Wang, D., and Cao, J.(2010). Fabrication and optical properties of Ce-doped ZnO nanorods. *Journal of Applied Physics* 107, 074302

Lim, T.C., Kotaki, M., Yong, T.K.J., Fujihara, K. and Ramakrishna, S. (2004). Recent advances in tissue engineering of electrospun nanofibers. *Mater. Technol.*, 19(1), pp. 20-27Liu, G.J., Qiao, LJ. and Guo, A. (1996). Diblock copolymer nanofibers. *Macromol.*, 29(16), pp. 5508-5510.

Liu, G.J., Ding, J.F., Qiao, L.J., Guo, A., Dyraov, B.P., Gleeson, J.T., Hashimoto, T. and Saijo, K. (1999). Polystyrene-block-poly (2-cinnamoylethyl methacrylate) nanofibers - Preparation, characterization, and liquid crystalline properties. *Chem. Eur. J.*, 5(9), pp. 2740-2749.

Ma, P.X. and Zhang, R. (1999). Synthetic nano-scale fibrous extracellular matrix. *J. Biomed. Mater. Res.*, 46(1), pp. 60-72.

Ondarcuhu, T. and Joachim, C. (1998). Drawing a single nanofibre over hundreds of microns. *Europhys. Lett.*, 42(2), pp. 215-220.

Pradhan, D and Leung, K. T. (2008). Controlled growth of two-dimensional and one-dimensional ZnO nanostructures on indium tin oxide coated glass by direct electrodeposition. *Langmiur* 24 (17) 9707-9716

Reneker, D. H., Yarin, A. L., Fong, H. and Koombhongse, S. (2000). Bending instability of electrically charged liquid jets of polymer solutions in electrospinning. *J. Appl. Phys.* 87, pp. 4531-4547.

Reneker, D.; Chun, I.(1996). Nanometer diameter fibers of polymer, produced by electrospinning. *Nanotechnology*, 7, 216-223.

Seeram Ramakrishna, Kazutoshi Fujihara, Wee-Eong Teo.Teik-Cheng Lim and Zuwei Ma, (2005) An Introduction to Electrospinning and Fibres. *World Scientific Publishing Co. Pte. Ltd.5 Ton Tuck Link, Singapore* 596224

Shan, F.K., Shin, B.C., Kim, S.C. and Yu, Y.S.,(2003). Substrate effect of ZnO thin films prepared by PLD. *J. Eur. Cerm. Soc.*

Shin, Y.; Hohman, M.; Brenner, M.; Rutledge, G. (2001). Experimental characterization of electrospinning: the electrically forced jet and instabilities. Polymer, 42, 9955- 9967.

Suthar, A. and Chase, G. (2001), Nanofiber in filter media. *Chemical Engineer*, December, pp. 26-28.

Yang, F., Murugan, R., Wang, S. and Ramakrishna, S. (2005). Electrospinning of nano/micro scale poly(L-lactic acid) aligned fibers and their potential in neural tissue engineering. *Biomaterials.* 26, pp. 2603-2610.

Yan, X.H., Liu, G.J., Liu, F.T., Tang, B.Z., Peng, H., Pakhomov, A.B. and Wong, C.Y. (2001). Superparamagnetic triblock copolymer/Fe203 hybrid nanofibers. *Angew. Chem. Int. Ed.*, 40(19), pp. 3593-3596.